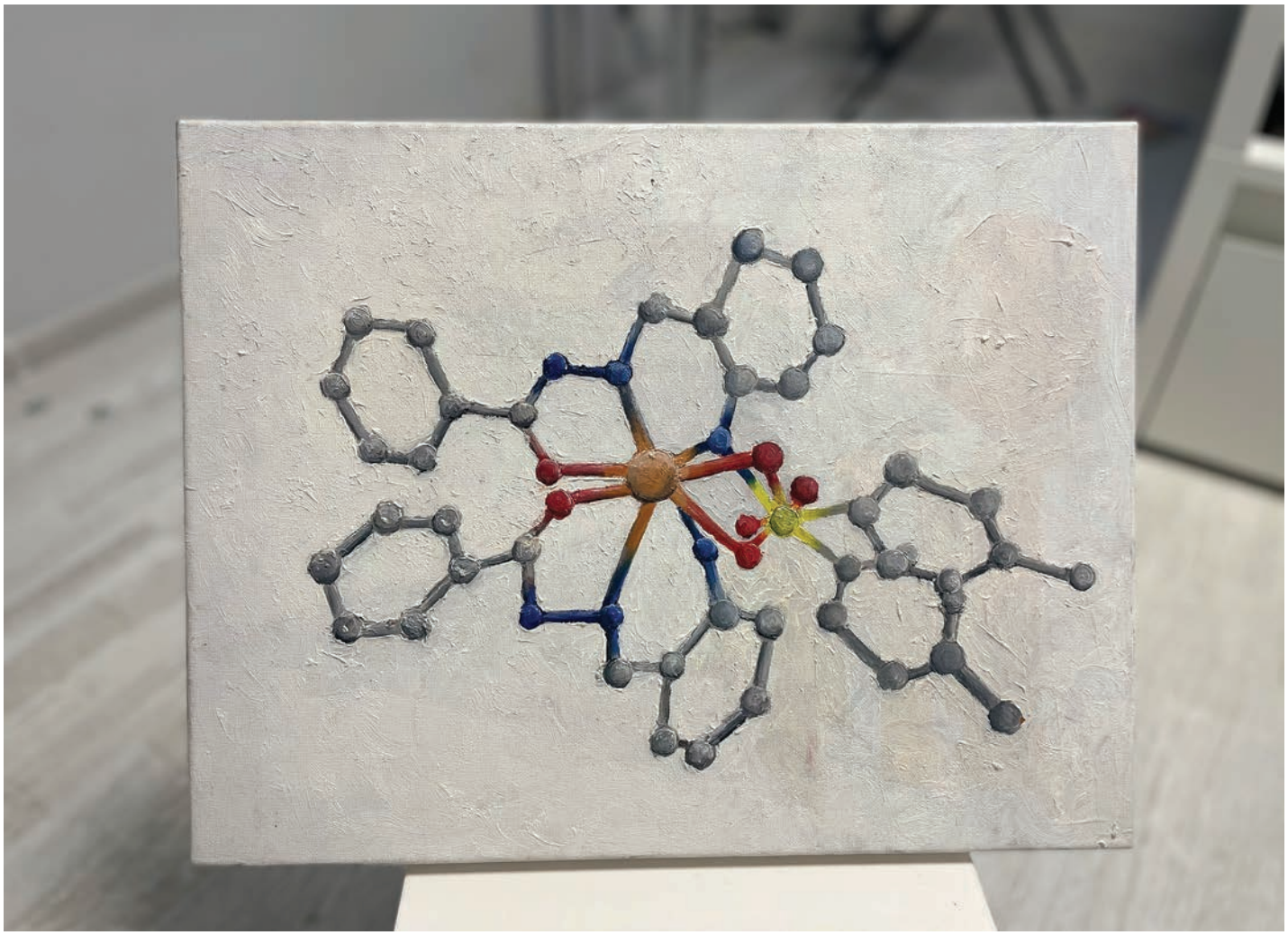

Showcasing research from DSc Valentina V. Utochnikova group, Chemistry Dept, Lomonosov Moscow State University, Russia, and Professor Stefan Bräse group, Organic Chemistry Institute, Karlsruhe Institute of Technology, Germany.

Highly NIR-emitting ytterbium complexes containing 2-(tosylaminobenzylidene)-*N*-benzoylhydrazone anions: structure in solution and use for bioimaging

Joint research of the groups of Valentina Utochnikova from the Lomonosov Moscow State University (Russia) and Stefan Bräse from the Karlsruhe Institute of Technology (Germany) is devoted to the design of novel luminescent materials for bioimaging. In the present paper, a novel highly NIR emissive ytterbium complex was obtained, the existence of which was predicted and corroborated using NMR spectroscopy determining its structure in solution. The obtained complex combined non-toxicity, high solubility, and stability in solution additionally to intense luminescence, which resulted in its successful use in NIR bioimaging.

Highly NIR-emitting ytterbium complexes containing 2-(tosylaminobenzylidene)-*N*-benzoylhydrazone anions: structure in solution and use for bioimaging†

Anton D. Kovalenko, [a,b] Alexander A. Pavlov, [c] Ilya D. Ustinovich,[c] Alena S. Kalyakina, [d] Alexander S. Goloveshkin,[c] Łukasz Marciniak, [e] Leonid S. Lepnev,[f] Anatolii S. Burlov,[g] Ute Schepers,[h,i] Stefan Bräse[i,j] and Valentina V. Utochnikova *[a,k]

Solution behaviour in DMSO using 1D and 2D NMR spectroscopy was performed for lanthanide complexes Ln(L)(HL) and $Ln(HL)_2Cl$, containing non-macrocyclic 2-(tosylamino)-benzylidene-*N*-benzoylhydrazone (H_2L), and the structure of $[Yb(L)]^+$ cation in solution was determined. Based on the NMR data, the possibility to obtain novel complexes containing $[Ln(L)_2]^-$ was predicted, which was successfully synthesized, and the crystal structure of $K(C_2H_5OH)_3[Yb(L)_2]$ was determined. Thanks to its high quantum yield of NIR luminescence (1.3 ± 0.2%), high absorption, low toxicity, and the stability of its anion against dissociation in DMSO, $K(H_2O)_3[Yb(L)_2]$ was successfully used for bioimaging.

[a]*Department of Material Sciences, Lomonosov Moscow State University, Moscow, Russian Federation. E mail: valentina.utochnikova@gmail.com*
[b]*Center for Molecular Biophysics, CNRS (UPR 4301), Orléans, France*
[c]*Nesmeyanov Institute of Organoelement Compounds of the Russian Academy of Sciences, Moscow, Russian Federation*
[d]*Institute of Biological and Chemical Systems (IBCS FMS), Karlsruhe Institute of Technology (KIT), Hermann von Helmholtz Platz 1, KarlsruheEggenstein Leopolddshafen, Germany*
[e]*Institute of Low Temperature and Structure Research, Polish Academy of Sciences, Wroclaw, Poland*
[f]*P.N. Lebedev Physical Institute RAN, Moscow, Russian Federation*
[g]*Institute of Physical and Organic Chemistry, Southern Federal University, Rostov on Don, Russian Federation*
[h]*Institute of Functional Interfaces (IFG), Karlsruhe Institute of Technology (KIT), Hermann von Helmholtz Platz 1, Eggenstein Leopolddshafen, Germany*
[i]*Institute of Organic Chemistry, Karlsruhe Institute of Technology (KIT), Karlsruhe, Germany*
[j]*Institute of Biological and Chemical Systems (IBCS FMS), Karlsruhe Institute of Technology (KIT), Hermann von Helmholtz Platz 1, KarlsruheEggenstein Leopolddshafen, Germany*
[k]*Department of Chemistry, Lomonosov Moscow State University, Moscow, Russia, Russian Federation*

†Electronic supplementary information (ESI) available. CCDC 2016985. For ESI and crystallographic data in CIF or other electronic format see DOI: 10.1039/d0dt03913f

Luminescent imaging, in comparison to other imaging technologies such as magnetic resonance imaging (MRI), computed tomography (CT), photoacoustic (PA), positron emission tomography (PET) and single-photon emission computed tomography (SPECT), has attracted extensive attention in biomedical studies due to its quick feedback, high sensitivity, non-hazardous radiation and low cost.[1–9] This technique enables the final images to be obtained within milliseconds and with a resolution of up to hundreds of nanometers using regular epifluorescence or confocal microscope, and can be lowered down to tens of nanometers for super-resolution techniques.[10,11] Attenuation of luminescence signals in biological samples can be correlated with the absorption and scattering of light by biological molecules like hemoglobin[12] and tissues like skin[13] and fat[14] which show strong absorptions in the visible (*vis*) and ultraviolet (UV) spectral regions. For these biomolecules and tissues, the scattering degree is inversely proportional to the absorbed wavelength, meaning that scattering decreases for longer wavelengths.[13,15–19] A combination of these two factors gives the range of 700–1700 nm in the near-infrared (NIR) spectral range, where luminescence signals have the lowest attenuation in biological samples.[20,21] These optical ranges are also named as NIR windows or biological transparency windows.[22]

Narrow emission bands of lanthanides significantly facilitate their signal detection, which makes them preferable over organic dyes.[23–27] Yb^{3+} with its emission peak at 980 nm, which belongs to the NIR biological window, is preferable for NIR bioimaging due to its rather high quantum yield comparing to Nd^{3+} or Er^{3+} complexes. This explains the undying interest in the investigating Yb^{3+}-activated NIR-emitting nanostructures for bioimaging.[28–31] Despite several effective Yb^{3+} compounds were obtained, *i.e.*[32–39] the problem of the obtaining of the efficient lanthanide-based NIR emitter is still far from being solved, which results from both low sensitization efficiency of NIR luminescence and ease of its quenching.

Recently we demonstrated a rather high efficiency of the NIR luminescence of ytterbium complexes with 2-(tosylamino)-benzylidene-*N*-(aryloyl)-hydrazones,[40–42] among which the quantum yields of Yb(L)(HL) and Yb(HL)$_2$Cl (aryloyl = benzoyl, *N*-[[2-(*p*-tolylsulfonylamino)-phenyl]-methyleneamino]-benzamide, Fig. 1) in powders reached 1.2% and 1.4%, correspondingly.[41] These values are high enough. For broadband NIR luminescence of organic dyes or d-metal complexes rather high quantum yields up to 11% were recorded.[43–46] However, for narrow emission of ytterbium such quantum yields are high in comparison with typical values of below 1%.[47–49] This has already allowed construction of an efficient Yb-emitting OLED,[42] and together with their crystal structure (complexes consist of monomers containing Ln^{3+} and two ligand anions) and independence of the quantum yield on the complex composition, *i.e.* ligand deprotonation degree, allows suggesting to further investigate the behaviour of these complexes for biological applications – and thus their properties must be studied in solutions.

To become promising candidates for bioimaging, these complexes must be stable against dissociation in solution. This became a reason why almost only Yb complexes with macrocyclic ligands, including porphyrine-based, are considered for bioimaging applications.[50–53] It was not therefore naturally expected that Yb(HL)$_2$Cl or Yb(L)(HL) complexes, containing rather small ligands, would not dissociate. To study complex solution behaviour, DMSO-d$_6$ solutions of complexes Lu(HL)$_2$Cl and Lu(L)(HL) of diamagnetic lutetium were investigated. A set of NMR spectra was recorded, including correlation spectroscopy (COSY), nuclear Overhauser effect spectroscopy (NOESY), heteronuclear single-quantum correlation spectroscopy (HSQC), heteronuclear multiple-bond correlation spectroscopy (HMBC) and diffusion ordered spectroscopy (DOSY) (see ESI† for details). Based on these data, all the ^{1}H and ^{13}C signals were assigned to corresponding nuclei (Fig. 1 and Table S1†). In the NMR spectra of Lu(HL)$_2$Cl in DMSO-d$_6$, there are two sets of signals with an equal integral intensity which correspond to the neutral ligand H_2L and $(L)^{2-}$ anion. It can be illustrated on the example of ^{1}H signals of –CH$_3$ (1), –CH N– (12) and amine NH protons (Fig. 1), which are singlets and do not overlap with other signals. No signals of expected $(HL)^-$ anion were detected. According to DOSY spectroscopy data, {H_2L} and {$(L)^{2-}$} ligand forms have significantly different diffusion coefficient, which, keeping in mind that H_2L and $(L)^{2-}$ have almost the same molecular weight, allows the assumption that in solution the $(L)^{2-}$ anion is bound by a lanthanide ion into a complex $[Lu(L)]^+$. This means that Lu(HL)$_2$Cl dissociates in DMSO with disproportionation of $(HL)^-$ into H_2L and $(L)^{2-}$, which is coordinated by the Ln^{3+} cation. This dissociation can be described using the following reaction (1):

$$Lu(HL)_2Cl = H_2L + [Lu(L)]^+ + Cl^- \quad (1)$$

In the NMR spectra of Lu(L)(HL) the signals of both H_2L and $[Lu(L)]^+$ are observed, as well as a group of signals of the other form of the double-charged anion $(L)^{2-}$. Based on DOSY spectroscopy data, this form of $(L)^{2-}$ also demonstrates a higher diffusion coefficient than of {H_2L} and similar to that of {$[Lu(L)]^+$}. This allows assuming that within this second form $(L)^{2-}$ is also coordinated by the lanthanide ion. Based on the stoichiometry of the reaction (2) of Lu(L)(HL) dissociation in DMSO-d$_6$, we can conclude the formation of a {$[Lu(L)_2]^-$} anionic complex:

$$2Lu(L)(HL) = H_2L + [Lu(L)]^+ + [Lu(L)_2]^- \quad (2)$$

The NMR spectroscopy data suggests the possibility of the formation of anionic complexes $[Ln(L)_2]^-$ and witnesses its stability in DMSO. This also indicates that the doubly charged $(L)^{2-}$ anion is more strongly coordinated by the lanthanide ion than the single-charged $(HL)^-$ anion.

To test this hypothesis, 1 eq. of KOH was added to the solution of Lu(L)(HL), and the resulting solution was subject to ^{1}NMR spectroscopy. Indeed, the NMR spectrum of the resulting solution lacked the ligand signals and only contained the signals of $[Lu(L)_2]^-$ (Fig. 2).

The determination of the $[Lu(L)_2]^-$ structure in solution is hampered by the presence of two non-equivalent ligands with overlapping proton signals. However, in the case of the cation $[Lu(L)]^+$ there is no other ligand, thus making it possible to determine the solution structure of the corresponding cation $[Yb(L)]^+$.

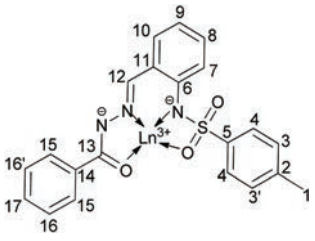

Fig. 1 Structural formula, atom numbering, and coordination of $(L)^{2-}$ anion.

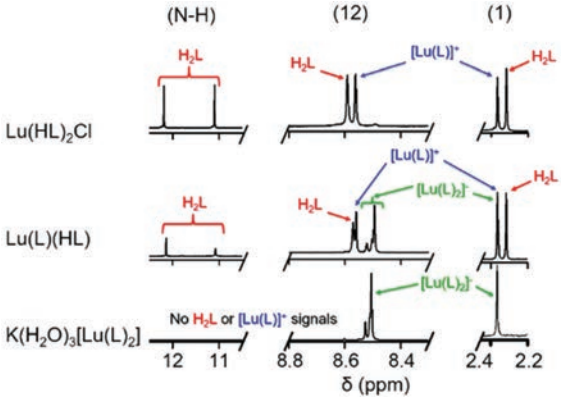

Fig. 2 Fragments of ^{1}H NMR spectra of the Lu(HL)$_2$Cl, Lu(L)(HL), and K(H$_2$O)$_3$[Lu(L)$_2$] in DMSO d$_6$ representing (1), (2) and N H protons signals. The full spectra are given in ESI.†

Due to the presence of unpaired electrons in lanthanide ions, the signals in the NMR spectra of complexes with paramagnetic ions can shift and broaden compared to the complexes with diamagnetic ions. The total observed shift (δ_{obs}) of the signal in the spectrum of the complex with a paramagnetic ion can be represented as the sum of the diamagnetic associated shift δ_D♦, Fermi-contact shift δ_{FC}♤, and pseudo contact shift δ_{PC}/:

$$\delta_{obs} = \delta_D + \delta_{FC} + \delta_{PC} \quad (3)$$

The Fermi-contact shift δ_{FC} [54]♣ is generally negligible for paramagnetic lanthanide ions compared to pseudo-contact shifts, so it is neglected for paramagnetic NMR shifts analysis.[55–57]

The pseudo contact shifts (δ_{PC}) arise from the dipole–dipole interaction of the magnetic moment of the resonating nucleus with the magnetic moment associated with the incompletely filled 4f-electron shell of the lanthanide cation.

The pseudo contact shift can be expressed in the spherical coordinate system (r, θ, φ) in terms of the axial $\Delta\chi_{ax}$ and rhombic $\Delta\chi_{rh}$ anisotropies of the magnetic susceptibility tensor χ if the coordinate system is associated with the eigenvectors of the tensor.

$$\delta_{PC} = \frac{1}{12\pi r^3}[\Delta\chi_{ax}(3\cos^2\theta \quad 1) + \frac{3}{2}\Delta\chi_{rh}3\sin^2\theta\cos^2 2\varphi] \quad (4)$$

The magnetic susceptibility tensor depends on the electronic configuration of the lanthanide ion.[58] Therefore, if the difference (δ_{obs}–δ_D) between the shifts in the spectra of complexes with paramagnetic (*i.e.* Yb^{3+}) and diamagnetic ions (*i.e.* Lu^{3+}) is known, it is possible to determine the coordinates of the atoms (r, θ, φ) that correspond to these signals, and, thus, to estimate the structure of the complex in solution. The determination of the structure of the ytterbium complex in a solution is additional proof of the ligand presence in solution in the coordinated form.

The values of pseudo contact shifts in the ^{1}H NMR spectrum were calculated for the $[Yb(L)]^+$ based on the fragment of the crystal structure of Yb(L)(HL), containing Yb ion and $(L)^{2-}$ ligand (Fig. 3a). The orientation of the magnetic susceptibility tensor, as well as its anisotropy values ($\Delta\chi_{ax}$ and $\Delta\chi_{rh}$), were varied to obtain the best convergence of the theoretical and experimental values of chemical shifts (δ_{calc} and δ_{exp}). The final values of δ_{calc} were plotted against δ_{exp}, showing perfect convergence (Fig. 3b). This means that the $[Yb(L)]^+$ fragment has the same structure in the DMSO solution as in the crystal.

This also indicates that the bonding of the lanthanide ion with the doubly charged anion $(L)^{2-}$ is stronger than with DMSO, and $[Ln(L)]^+$ is stable and does not dissociate even in a solution of such a strongly donor solvent is dimethylsulfoxide. Also, it gives every reason to assume that the anionic fragments $[Ln(L)_2]^-$ are also stable in solution.

Complexes containing $[Ln(L)_2]^-$ anions, predicted by NMR spectroscopy, were obtained preparatively by the interaction of Ln(L)(HL) (Ln = Yb, Lu) with KOH in ethanol:

$$Ln(L)(HL) + KOH + 2H_2O \rightarrow K(H_2O)_3[Ln(L)_2] \quad (5)$$

Its composition and structure were ascribed based of the TGA with mass-spectroscopy data, confirmed by elemental analysis data, and supported by IR spectroscopy (see ESI† for more details). Due to its ionic structure, complex $K(H_2O)_3[Ln(L)_2]$ demonstrates better solubility in polar solvents than both Ln(HL)Cl and Ln(L)(HL).

Single crystal of $K(C_2H_5OH)_3[Yb(L)_2]$ was obtained from ethanol, and its crystal structure was determined (Fig. 4). Despite the single crystal contains ethanol molecules coordinated to K^+, powders of $K(H_2O)_3[Ln(L)_2]$ contain water according to both thermal and elemental analyses. According to single-crystal XRD data, complex $K(C_2H_5OH)_3[Ln(L)_2]$ possesses monomeric structure, three ethanol molecules are coordinated by the K^+ ion, while ytterbium coordinates two L^{2-} ligands. The coordination environment of Yb^{3+} consists of four nitrogen atoms and four oxygen atoms, resulting in a CN of 8 (4O + 4N). Two nitrogen atoms and two oxygen atoms of the same ligand anion, coordinated to Yb^{3+}, forming a dis-

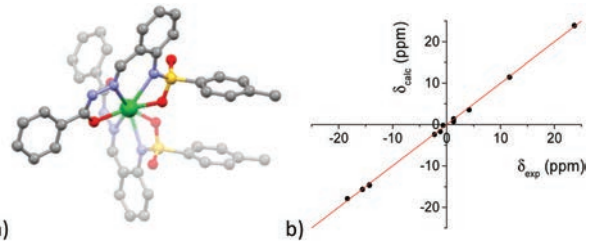

Fig. 3 (a) Structure of the $[Yb(L)]^+$ fragment in a DMSO solution (from cif file). (b) Experimental (δ_{exp}) *vs.* calculated (δ_{calc}) shifts in the NMR spectrum of the $[YbL]^+$ cation (black dots) and a straight line with a slope of 45° (red line).

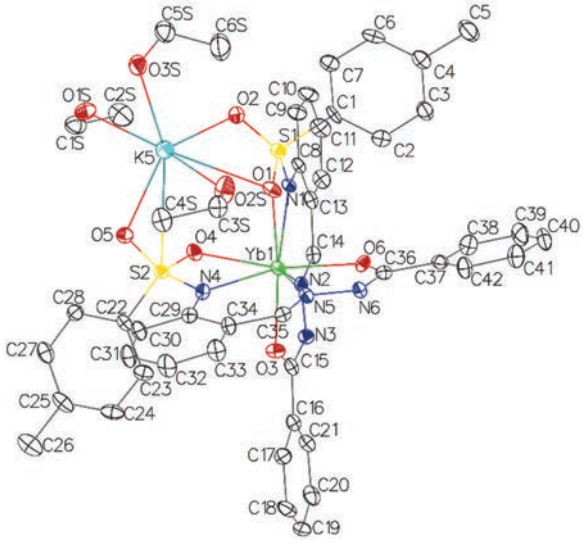

Fig. 4 Structure of $K(C_2H_5OH)_3[Yb(L)_2]$ (*P*1, *R* = 4.3%; atoms are rep resented by thermal displacement ellipsoids, hydrogen atoms are omitted for clarity).

torted trapezium; two distorted trapezia formed by the donor atoms of two anions of ligands in one mononuclear fragment are orthogonal to each other. As a result, in one mononuclear fragment, the benzylidene-*N*-benzoylhydrazone fragments are located almost orthogonally to each other. The same coordination environment of Ln^{3+} was earlier observed in Yb(HL)(L)$(EtOH)_2(H_2O)$, Yb(HL)(L)$(H_2O)_2$Lu$(HL)_2$Cl, and Er(L)(HL),[40] as well as in Yb$(L^1)(HL^1)$(EtOH) (H_2L^1 = 2-tosylaminobenzylidene-pyridyloylhydrazone).[42]

Powders of K$(H_2O)_3$[Ln$(L)_2$] (Ln = Yb, Lu) were studied by powder XRD. The obtained powder patterns were indexed and refined, proving the formation of individual compounds (Fig. 5). Though the obtained powder patterns could not be described by the single crystal, which is obvious due to the different solvent composition, the unit cell of single-crystal and powder have similarities, *i.e.* the same space group and comparable cell parameters (Table 1). It could be noted that cell volume of powder is less than that of a single crystal due to the substitution of ethanol molecules with water.

A rather high solubility of K$(H_2O)_3$[Yb$(L)_2$], as well as expected stability of $[Ln(L)_2]^-$ against dissociation, makes K$(H_2O)_3$[Yb$(L)_2$] interesting for luminescence bioimaging applications. Therefore, luminescent properties and cytotoxicity of K$(H_2O)_3$[Yb$(L)_2$] were investigated. It exhibited intense NIR luminescence of Yb^{3+} ion with a quantum yield determined to be 1.3%, able to be excited by visible light with $\lambda < 430$ nm (Fig. S6 and S10†). The analysis of the luminescent data (section "Luminescence spectroscopy" in ESI†) demonstrates that the internal quantum yield $Q_{Yb}^{Yb} = \frac{\tau_{obs}}{\tau_{rad}} = 1.4\%$, meaning that the sensitization efficiency equals 90%. Important is that usually positively charged molecules demonstrate better cell permeability,[59] however, small negatively charged molecules demonstrate better cell entry due to different pathway of cell entry.[60]

The molar extinction coefficient of K$(H_2O)_3$[Yb$(L)_2$] in DMSO reached 44 400 M^{-1} cm^{-1}. This together with the high quantum yield resulted in the intense photoluminescence of K$(H_2O)_3$[Yb$(L)_2$]. Important is that the quantum yield of K$(H_2O)_3$[Yb$(L)_2$] coincided within the experimental error (±0.2%) with those previously published for Yb$(HL)_2$Cl and Yb(L)(HL),[41] which probably results from the same ligand and Yb coordination environment.

Determination of the cytotoxicity of K$(H_2O)_3$[Yb$(L)_2$] in DMSO (Fig. S7†) showed LD50 value of 0.05 ± 0.01 g l^{-1}, and the safe concentration (cell survival >80%) of 0.02 g l^{-1}, which is sufficient for the use in living systems.

Table 1 Cell parameters obtained from single crystal and powder X ray diffraction

	Single crystal of K$(EtOH)_3$[Yb$(L)_2$]	Powder of K$(H_2O)_3$[Yb$(L)_2$]
a, Å	9.2427(13)	9.5889(10)
b, Å	11.0807(15)	10.2406(9)
c, Å	24.563(3)	22.663(2)
α, °	86.803(2)°	82.311(6)
β, °	88.788(2)°	89.542(7)
γ, °	74.750(2)°	70.884(6)
V, Å^3	2423.2(6)	2082.3(4)

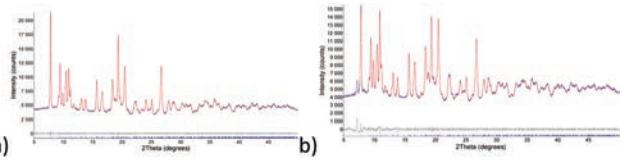

Fig. 5 The experimental (blue curve) and calculated (red curve) powder patterns and their difference (grey curve). Blue ticks indicated calculated positions of refined cell: (a) K$(H_2O)_3$[Yb$(L)_2$], (b) K$(H_2O)_3$[Lu$(L)_2$].

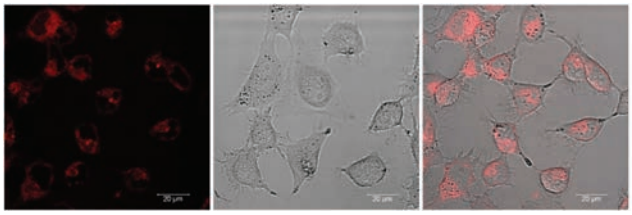

Fig. 6 Confocal images of non toxic K$(H_2O)_3$[Yb$(L)_2$] solution (DMSO, 5 mg g l^{-1}): luminescent channel (left), optical channel (mid), overlap (right).

The cell permeability and *in cellulo* luminescence of the complex were estimated in the visible range in the absence of the detector in the micron-range attached to the confocal microscope. The visible emission band in the spectrum of K$(H_2O)_3$[Yb$(L)_2$] is negligible (Fig. S8†); thus the appearance of the luminescence signal corresponding to this band inevitably signifies that NIR emission will also be bright.

The confocal microscopy data (Fig. 6) show that the complex penetrates the cells with no specific localization and avoids cell nuclei, being another example of cell-penetrating negatively-charged species. This allows recommending K$(H_2O)_3$[Yb$(L)_2$] as a material for bioimaging.

Thus, based on 1D and 2D NMR data, the dissociation of lanthanide complexes Lu$(HL)_2$Cl and Lu(L)(HL) in DMSO was described according to the reactions (1) and (2), and the structure of the cationic complex $[Yb(L)]^+$ in DMSO solution was determined. 1D and 2D NMR data further allowed a prediction of novel complexes K$(H_2O)_3$[Ln$(L)_2$] (Ln = Yb, Lu), which were successfully obtained, with anions $[Ln(L)_2]^-$ stable in DMSO against dissociation. The single-crystal structure of K$(C_2H_5OH)_3$[Yb$(L)_2$] was determined. High quantum yield (1.3 ± 0.2%) and high absorption (44 400 M^{-1} cm^{-1}) of K$(H_2O)_3$[Yb$(L)_2$] together with $[Yb(L)_2]^-$ stability in DMSO allowed to recommend it as a promising candidate for luminescence bioimaging. Preliminary *in cellulo* experiments revealed low toxicity and cell permeability of K$(H_2O)_3$[Yb$(L)_2$].

Conflicts of interest

There are no conflicts to declare.

Acknowledgements

Synthesis, Characterization and Bioimaging were supported by RSF (#20-53-10073). NMR measurements were supported by RSF (# 20-73-00194). PL studies were supported by Prezident's grant (MD-2821.2021.1.3). X-ray diffraction studies were performed with the financial support from Ministry of Science and Higher Education of the Russian Federation using the equipment of Center for molecular composition studies of INEOS RAS. The Deutsche Forschungsgemeinschaft under Germany's Excellence Strategy 3DMM2O—EXC-2082/1–390761711 and the DFG-funded Collaborative Research Centre (SFB) TRR 88/3MET "Cooperative Effects in Homo- and Heterometallic Complexes" are gratefully acknowledged.

Notes and references

1 L. Yuan, W. Lin, K. Zheng and S. Zhu, *Acc. Chem. Res.*, 2013, **46**, 1462–1473.
2 Q. Xiao, H. Zhu, D. Tu, E. Ma and X. Chen, *J. Phys. Chem. C*, 2013, **117**, 10834–10841.
3 X. Li, X. Gao, W. Shi and H. Ma, *Chem. Rev.*, 2014, **114**, 590–659.
4 L. A. Sordillo, Y. Pu, S. Pratavieira, Y. Budansky and R. R. Alfano, *J. Biomed. Opt.*, 2014, **19**, 056004.
5 H. Dong, L. D. Sun and C. H. Yan, *Chem. Soc. Rev.*, 2015, **44**, 1608–1634.
6 V. S. R. Harrison, C. E. Carney, K. W. MacRenaris, E. A. Waters and T. J. Meade, *J. Am. Chem. Soc.*, 2015, **137**, 9108–9116.
7 Y. Sun, X. Ma, K. Cheng, B. Wu, J. Duan, H. Chen, L. Bu, R. Zhang, X. Hu, Z. Deng, L. Xing, X. Hong and Z. Cheng, *Angew. Chem., Int. Ed.*, 2015, **54**, 5981–5984.
8 B. Del Rosal, I. Villa, D. Jaque and F. Sanz-Rodríguez, *J. Biophotonics*, 2016, **9**, 1059–1067.
9 Y. Wei, X. Yang, Y. Ma, S. Wang and Q. Yuan, *Chin. J. Chem.*, 2016, **34**, 558–569.
10 G. Hong, J. T. Robinson, Y. Zhang, S. Diao, A. L. Antaris, Q. Wang and H. Dai, *Angew. Chem., Int. Ed.*, 2012, **51**, 9818–9821.
11 M. Bates, B. Huang, G. T. Dempsey and X. Zhuang, *Science*, 2007, **317**, 1749–1753.
12 M. Friebel, J. Helfmann, U. Netz and M. Meinke, *J. Biomed. Opt.*, 2009, **14**, 034001.
13 A. N. Bashkatov, E. A. Genina, V. I. Kochubey and V. V. Tuchin, *J. Phys. D: Appl. Phys.*, 2005, **38**, 2543–2555.
14 R. L. P. van Veen, H. J. C. M. Sterenborg, A. Pifferi, A. Torricelli and R. Cubeddu, *The Optical Society*, 2014, p. SF4.
15 W. Zhu, *Sci. China: Chem.*, 2016, **59**, 203–204.
16 T. Zako, M. Yoshimoto, H. Hyodo, H. Kishimoto, M. Ito, K. Kaneko, K. Soga and M. Maeda, *Biomater. Sci.*, 2015, **3**, 59–64.
17 J. Zhao, D. Zhong and S. Zhou, *J. Mater. Chem. B*, 2018, **6**, 349–365.
18 A. N. Bashkatov, E. A. Genina and V. V. Tuchin, *J. Innovative Opt. Health Sci.*, 2011, **4**, 9–38.
19 K. Welsher, S. P. Sherlock and H. Dai, *Proc. Natl. Acad. Sci. U. S. A.*, 2011, **108**, 8943–8948.
20 A. M. Smith, M. C. Mancini and S. Nie, *Nat. Nanotechnol.*, 2009, **4**, 710–711.
21 G. Hong, A. L. Antaris and H. Dai, *Nat. Biomed. Eng.*, 2017, **1**, 0010.
22 R. Weissleder and V. Ntziachristos, *Nat. Med.*, 2003, **9**, 123–128.
23 D. C. Rodriguez Burbano, R. Naccache and J. A. Capobianco, in *Handbook on the Physics and Chemistry of Rare Earths*, Elsevier B.V., 1st edn, 2015, vol. 47, pp. 273–347.
24 X. Wang, H. Chang, J. Xie, B. Zhao, B. Liu, S. Xu, W. Pei, N. Ren, L. Huang and W. Huang, *Coord. Chem. Rev.*, 2014, **273–274**, 201–212.
25 A. J. Amoroso and S. J. A. Pope, *Chem. Soc. Rev.*, 2015, **44**, 4723–4742.
26 J.-C. G. Bünzli, *J. Lumin.*, 2016, **170**, 866–878.
27 J. C. G. Bünzli, in *Luminescence of Lanthanide Ions in Coordination Compounds and Nanomaterials*, Wiley Blackwell, 2014, vol. 9781119950837, pp. 125–196.
28 H. Wang, X. Mu, J. Yang, Y. Liang, X. D. Zhang and D. Ming, *Coord. Chem. Rev.*, 2019, **380**, 550–571.
29 Y. Ning, M. Zhu and J. L. Zhang, *Coord. Chem. Rev.*, 2019, **399**, 213028.
30 H. Wan, H. Du, F. Wang and H. Dai, *Adv. Funct. Mater.*, 2019, **29**, 1900566.
31 Q. Miao and K. Pu, *Adv. Mater.*, 2018, **30**(49), 1801778.
32 S. V. Fedorenko, O. D. Bochkova, A. R. Mustafina, V. A. Burilov, M. K. Kadirov, C. V. Holin, I. R. Nizameev, V. V. Skripacheva, A. Y. Menshikova, I. S. Antipin and A. I. Konovalov, *J. Phys. Chem. C*, 2010, **114**, 6350–6355.
33 A. Foucault-Collet, K. A. Gogick, K. A. White, S. Villette, A. Pallier, G. Collet, C. Kieda, T. Li, S. J. Geib, N. L. Rosi and S. Petoud, *Proc. Natl. Acad. Sci. U. S. A.*, 2013, **110**, 17199–17204.
34 X. Feiyun, E. H. Song, S. Ye and Q. Y. Zhang, *J. Alloys Compd.*, 2014, **587**, 177–182.
35 M. Yagoub, H. Swart, P. Bergman and E. Coetsee, *AIP Adv.*, 2016, **6**, 25204.
36 X. Ge, Z. M. Song, L. Sun, Y. F. Yang, L. Shi, R. Si, W. Ren, X. Qiu and H. Wang, *Biomaterials*, 2016, **108**, 35–43.
37 E. Mathieu, A. Sipos, E. Demeyere, D. Phipps, D. Sakaveli and K. E. Borbas, *Chem. Commun.*, 2018, **54**, 10021–10035.
38 Y. Li, S. Zeng and J. Hao, *ACS Nano*, 2019, **13**, 248–259.
39 F. Wu, H. Su, X. Zhu, K. Wang, Z. Zhang and W. K. Wong, *J. Mater. Chem. B*, 2016, **4**, 6366–6372.
40 A. D. Kovalenko, I. S. Bushmarinov, A. S. Burlov, L. S. Lepnev, E. G. Ilina and V. V. Utochnikova, *Dalton Trans.*, 2018, **47**, 4524–4533.
41 V. V. V. Utochnikova, A. D. D. Kovalenko, A. S. S. Burlov, L. Marciniak, I. V. V. Ananyev, A. S. S. Kalyakina, N. A. A. Kurchavov and N. P. P. Kuzmina, *Dalton Trans.*, 2015, **44**, 12660–12669.

42 A. Kovalenko, P. O. Rublev, L. O. Tcelykh, A. S. Goloveshkin, L. S. Lepnev, A. S. Burlov, A. A. Vashchenko, Ł. Marciniak, A. M. Magerramov, N. G. Shikhaliyev, S. Z. Vatsadze and V. V. Utochnikova, *Chem. Mater.*, 2019, **31**, 759–773.

43 M. H. Liu, T. C. Chen, J. R. Vicente, C. N. Yao, Y. C. Yang, C. P. Chen, P. W. Lin, Y. C. Ho, J. Chen, S. Y. Lin, Y. H. Chan, Y. H. Chan and Y. H. Chan, *ACS Appl. Bio Mater.*, 2020, **3**, 3846–3858.

44 G. Chen, C. Yang and P. N. Prasad, *Acc. Chem. Res.*, 2013, **46**, 1474–1486.

45 K. Gu, Y. Xu, H. Li, Z. Guo, S. Zhu, S. Zhu, P. Shi, T. D. James, H. Tian and W. H. Zhu, *J. Am. Chem. Soc.*, 2016, **138**, 5334–5340.

46 H. Lv, X. F. Yang, Y. Zhong, Y. Guo, Z. Li and H. Li, *Anal. Chem.*, 2014, **86**, 1800–1807.

47 S. Biju, N. Gopakumar, J.-C. G. Bunzli, R. Scopelliti, H. K. Kim and M. L. P. Reddy, *Inorg. Chem.*, 2013, 8750–8758.

48 V. A. Ilichev, A. V. Rozhkov, R. V. Rumyantcev, G. K. Fukin, I. D. Grishin, A. V. Dmitriev, D. A. Lypenko, E. I. Maltsev, A. N. Yablonskiy, B. A. Andreev and M. N. Bochkarev, *Dalton Trans.*, 2017, **46**, 3041–3050.

49 E. R. Trivedi, S. V. Eliseeva, J. Jankolovits, M. M. Olmstead, S. Petoud and V. L. Pecoraro, *J. Am. Chem. Soc.*, 2014, **136**, 1526–1534.

50 W. D. Horrocks, J. P. Bolender, W. D. Smith and R. M. Supkowski, *J. Am. Chem. Soc.*, 1997, **119**, 5972–5973.

51 X.-S. Ke, B.-Y. Yang, X. Cheng, S. L.-F. Chan and J.-L. Zhang, *Chem. – Eur. J.*, 2014, **20**, 4324–4333.

52 J.-Y. Hu, Y. Ning, Y.-S. Meng, J. Zhang, Z.-Y. Wu, S. Gao and J.-L. Zhang, *Chem. Sci.*, 2017, **8**, 2702–2709.

53 C. S. Bonnet, F. Buron, F. Caillé, C. M. Shade, B. Drahoš, L. Pellegatti, J. Zhang, S. Villette, L. Helm, C. Pichon, F. Suzenet, S. Petoud and É. Tóth, *Chem. – Eur. J.*, 2012, **18**, 1419–1431.

54 J. A. Peters, *J. Magn. Reson.*, 1986, **68**, 240–251.

55 B. Bleaney, *J. Magn. Reson.*, 1972, **8**, 91–100.

56 N. Ishikawa, *J. Phys. Chem. A*, 2003, **107**, 5831–5835.

57 N. Ishikawa, M. Sugita, T. Okubo, N. Tanaka, T. Iino and Y. Kaizu, *Inorg. Chem.*, 2003, **42**, 2440–2446.

58 G. Otting, *Annu. Rev. Biophys.*, 2010, **39**, 387–405.

59 I. Martín, M. Teixidó and E. Giralt, *ChemBioChem*, 2011, **12**(6), 896–903.

60 C. P. Montgomery, B. S. Murray, E. J. New, R. Pal and D. Parker, *Acc. Chem. Res.*, 2009, **42**(7), 925–937.